

POTENTIAL ENERGY SURFACE IN NUCLEUS–NUCLEUS COLLISIONS CORRECTED FOR EXACT NUCLEAR MASSES

L. SHVEDOV, J. BŁOCKI, AND J. WILCZYŃSKI

The Andrzej Sołtan Institute for Nuclear Studies
05-400 Otwock-Świerk, Poland

(Received October 8, 2002)

Dedicated to Adam Sobiczewski in honour of his 70th birthday

A macroscopic model for calculating potential energy for nuclear shapes relevant in fusion and fission processes is presented. The potential energy is calculated as the sum of the Yukawa-plus-exponential folding potential and the Coulomb energy assuming realistic, diffuse charge distributions. Shape independent components (*e.g.* the Coulomb exchange and Wigner terms) in the Krappé–Nix–Sierk formulae for the total energy were combined and adjusted to the experimental ground state masses of the compound nucleus (for the mononuclear regime), and two separated nuclei (for the binary regime), and assumed to change in the transition region between these two regimes. We have used experimental data on heights of the saddle point (experimental fission barriers) and the interaction barrier (experimentally deduced fusion barriers) to verify our model calculations. Very good agreement with the fission barrier data proved correctness of our description of the shell-correction energies. Predictions of the interaction barriers also agree very well with experimental data. The calculated interaction barriers are significantly lower than those predicted with the “proximity potential”, and agree with the experimentally deduced fusion barriers.

PACS numbers: 25.85.–w, 25.70.Jj

1. Introduction

Good knowledge of the potential energy of a given nuclear system in the multidimensional space of deformation degrees of freedom is essential for realistic description of the dynamics of heavy ion collisions. In our previous calculations [1], potential energy was taken as the sum of the Coulomb and nuclear components, the latter calculated using the Yukawa-plus-exponential

potential [2]. In addition, shell-correction energies were also taken into account. We found them to be crucial for reproducing experimental fission barriers.

In the previous paper [1] we focused our analysis on the determination of fission barriers in heavy nuclei, defined as the energy of the saddle point relative to the ground-state of the compound nucleus. In the present work we aimed additionally at constructing the potential energy surface for describing nucleus-nucleus collisions, for which the reference level of the ground-state energy of the compound nucleus is less convenient. We have chosen therefore the energy of two colliding nuclei in their ground states (*i.e.* at the infinite relative distance) as the reference level. Potential energy for the mononuclear shape (calculated without constant terms, independent of deformation) was matched to exact value of the ground-state mass (experimental or theoretical) of the compound nucleus, and similarly, the calculated potential energy of two separated nuclei at the infinite distance was matched to the sum of their ground-state masses. In this approach both, the experimental fission barriers and the entrance-channel fusion barriers were used for verifying correctness of our calculations.

2. Parametrization of nuclear shapes

We assume shapes which are axially symmetric and consisting of two spheres of radii R_1 and R_2 connected smoothly by a portion of a quadratic surface of revolution [3]. For the volume conserving shapes there are three variables defining the shape completely (see Fig. 1):

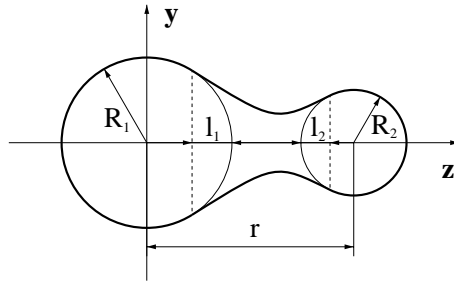


Fig. 1. Axially symmetric shape of a di-nuclear system, and the definition of the parameters determining the variables ρ , λ and Δ in Eqs (1)–(3).

$$\text{Distance variable} \quad \rho = r/(R_1 + R_2), \quad (1)$$

$$\text{Deformation or neck variable} \quad \lambda = (l_1 + l_2)/(R_1 + R_2), \quad (2)$$

$$\text{Asymmetry variable} \quad \Delta = (R_1 - R_2)/(R_1 + R_2). \quad (3)$$

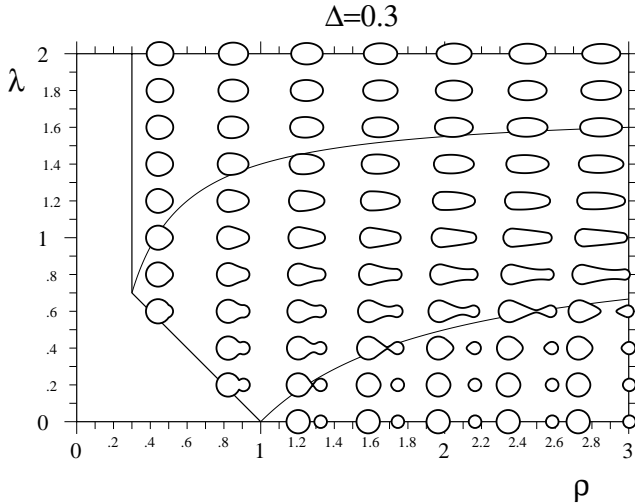


Fig. 2. Shapes of a nuclear system for a fixed asymmetry $\Delta = 0.3$, plotted as a function of the distance variable ρ and the deformation or neck variable λ . The compound-nucleus sphere corresponds to the locus $\rho = \Delta = 0.3$. Scission line is given by the equation $\lambda = 1 - (1/\rho)$.

In Fig. 2 we present shapes as a function of ρ and λ for a fixed value of $\Delta = 0.3$, that corresponds to the ratio of mass numbers of the colliding nuclei equal to 6.4.

3. Calculations of the potential energy

Potential energy of a nuclear system is calculated as the sum of the macroscopic and microscopic components:

$$E(Z, N, \text{shape}) = E_{\text{macr}}(Z, N, \text{shape}) + E_{\text{micr}}(Z, N, \text{shape}). \quad (4)$$

The macroscopic component of the potential energy is the sum of the nuclear potential taken as the folding potential of the Yukawa-plus-exponential two-body interaction [2] and the Coulomb potential calculated for the diffuse charge distribution [4]. The microscopic component is the shell correction to the potential energy. For the equilibrium shapes, the shell correction is taken as for the ground state, and is read from the Thomas–Fermi mass tables of Myers and Swiatecki [5]. These ground-state shell corrections are then attenuated with the increasing deformation according to a phenomenological formula proposed by Myers and Swiatecki in Ref. [6]. For more details concerning calculations of all the components of the potential energy $E(Z, N, \text{shape})$ see Ref. [1].

Special care is necessary in accounting for *shape-independent* components (for example, the Coulomb exchange term and the Wigner term) in the Krappe–Nix–Sierk formulae used in our calculations. By requiring adjustment of the calculated potential energy of the fused system to the ground-state mass of the compound nucleus, and the adjustment of the calculated potential energy of two separated nuclei at the infinite distance to the sum of their ground-state masses, we have introduced the correction term to Eq. (4) that reads:

$$E_{\text{tot}}(Z, N, \text{shape}) = E(Z, N, \text{shape}) + (\Delta M_0 c^2 - \Delta E_0(Z, N))f(\text{shape}), \quad (5)$$

where $\Delta M_0 = M_{\text{cn}} - M_1 - M_2$ is the difference of the experimental ground-state mass of the compound nucleus, M_{cn} , and the ground-state masses of the projectile and target nuclei, M_1 and M_2 , and $\Delta E_0(Z, N)$ is the respective difference of the *calculated* potential energy of the compound sphere and the *calculated* energies of the projectile and target nuclei.

A value of the form factor $f(\text{shape})$ must be 1 for the fused compound nucleus and 0 for two separated nuclei. In between, it should smoothly change in the transition from the mononuclear to dinuclear regime. We assumed that the form factor f is scaled by the opening of the neck between the two nuclei. Definite functional form and parametrization of f was chosen by attempting to reproduce experimental values of fission barriers, and — at the same time — the entrance-channel fusion barriers. This procedure led us to the following form of f :

$$f(\text{shape}) = \sin^2 \left(k \frac{\pi}{2} \frac{r_{\text{neck}}}{R_{\text{cn}}} \right), \quad (6)$$

where r_{neck} is an effective radius of the neck at a given distance between the two nuclei calculated as proposed in Ref. [7], R_{cn} is the radius of the compound nucleus, and k is a parameter determining how steep is the transition of the shape-independent component of the mass formula from the dinuclear to the mononuclear regime. By fitting both, the fission barriers and fusion barriers deduced from experimental data, we have determined a value of k to be $k = 1.6$. As it is seen from Fig. 3, for this value of k , the transition region (where f changes its value from 0 to 1) is relatively narrow in the plane of (ρ, λ) coordinates, and is located just around the scission line.

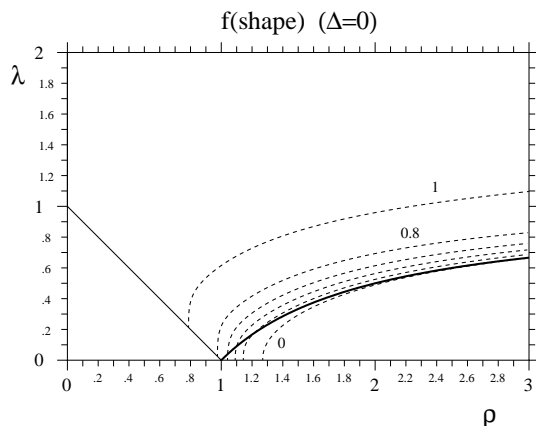


Fig. 3. Localization in the (ρ, λ) plane of the transition region, where the form factor f , given by Eq. (6), changes its value from 0 to 1. It is seen that the ‘structural’ energy associated with the ground-state mass correction in Eq. (5) rapidly dissolves in vicinity of the scission line.

4. Results

In Fig. 4 we present an example of a contour plot of the potential energy for a symmetric ($\Delta = 0$) nuclear system that combines to the ^{208}Pb

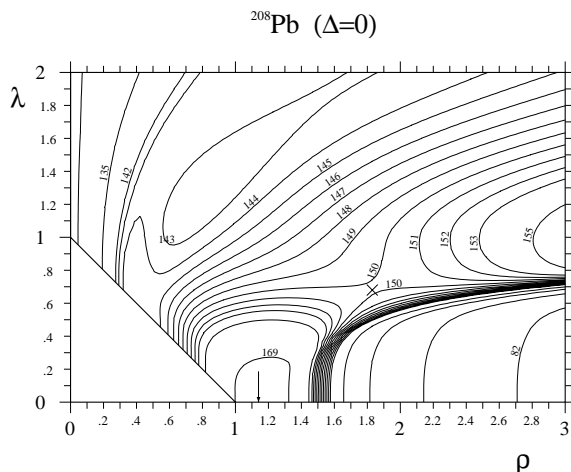


Fig. 4. Potential energy surface for a symmetric $\Delta = 0$ nuclear system that combines to ^{208}Pb compound nucleus. Modulation of a strong shell effect with increasing elongation ρ is clearly seen. At the saddle point (cross), the shell effect is already completely washed out. Viewing the system from the entrance channel (a hypothetical $^{104}_{41}\text{Nb} + ^{104}_{41}\text{Nb}$ reaction), one can see a maximum of the potential energy along the line $\lambda = 0$, indicated by an arrow, and representing the entrance-channel interaction barrier.

compound nucleus. One can read from such a plot the height of the fission barrier, *i.e.*, the potential energy of the saddle point (indicated in Fig. 4 by a cross), taken relative to the ground-state energy of the compound nucleus (corresponding to the locus $\rho = \Delta = 0$ in Fig. 4). On the other hand, one can read also the height of the entrance-channel barrier (indicated in Fig. 4 by an arrow) that in the discussed example refers to a hypothetical collision of two ${}_{41}^{104}\text{Nb}$ nuclei.

4.1. Saddle point energies (fission barriers)

We have applied our model for systematic calculations of fission-barriers for about 120 nuclei in the range of atomic numbers $71 \leq Z \leq 100$, for which the fission barriers had been deduced from experimental data [8–10]. Position of the saddle point in the (ρ, λ) plane was determined for each nucleus and the saddle-point energy was calculated with respect to the ground state. Results of these calculations are summarized in Fig. 5, where the calculated and experimental fission barriers are compared. It is seen that the

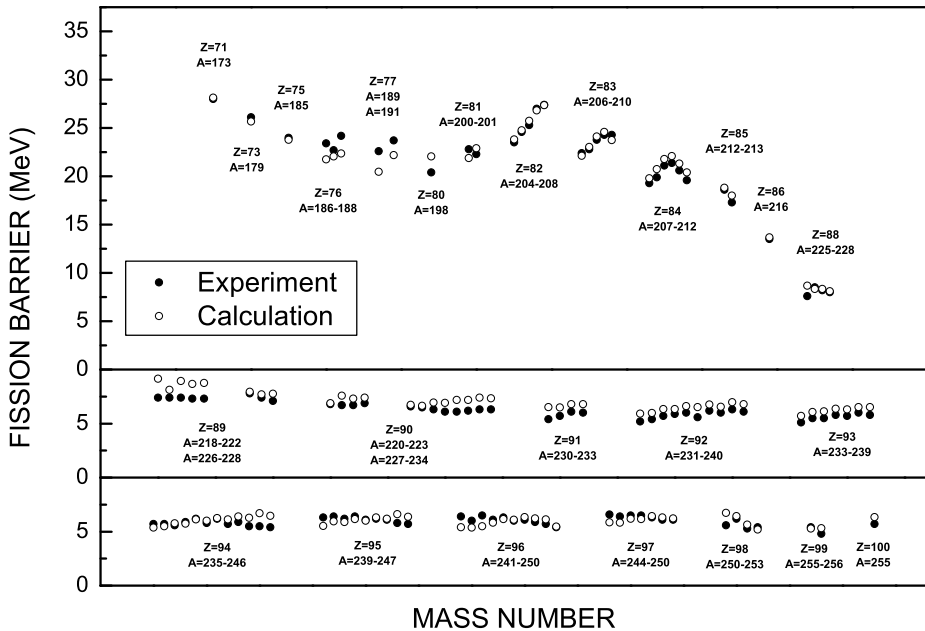


Fig. 5. Comparison of experimental fission barriers [8–10] with results of present calculations.

agreement between our predictions and experimental values is quite good. The RMS deviation for the whole set of 120 nuclei is 0.72 MeV. One can see also that the individual pattern in the dependence of the fission barrier

on A and Z is very well reproduced for the whole range of studied nuclei. Figure 5 shows also that for heavy nuclei of $Z > 90$, the fission barriers stabilize at almost constant level of about 5 MeV. This is the consequence of the decreasing macroscopic component of the fission barrier for transuranic nuclei (practically to zero for $Z \geq 100$) and thus the increasing role of the ground-state shell-correction energy that ultimately remains the only factor responsible for non-vanishing fission barriers in super-heavy nuclei.

4.2. Entrance-channel barriers

As mentioned in Sec. 3, the potential energy in vicinity of the scission line is sensitive to structural properties (ground-state masses and shell effects) of two separated nuclei. The calculated entrance-channel barriers in the potential energy depend on these structural properties of the projectile and target nuclei, and can be compared with the fusion barriers determined experimentally.

Experimental values of the fusion barrier can be deduced from very precise measurements of the energy dependence of the fusion cross section σ_{fus} at near-barrier and sub-barrier energies. As shown in Ref. [11], the second derivative of the product of the cross section times energy, $d^2(E\sigma_{\text{fus}})/dE^2$, describes the barrier distribution. Thus the average value of the distribution can be compared with the interaction barrier calculated theoretically.

In Fig. 6 we give an example of the experimental information on the distribution of the fission barrier $d^2(E\sigma_{\text{fus}})/dE^2$, obtained in Ref. [12] for the $^{16}\text{O} + ^{144}\text{Sm}$ reaction. In order to make comparisons with our theoretical predictions, we fit the $d^2(E\sigma_{\text{fus}})/dE^2$ distribution for a given reaction with a

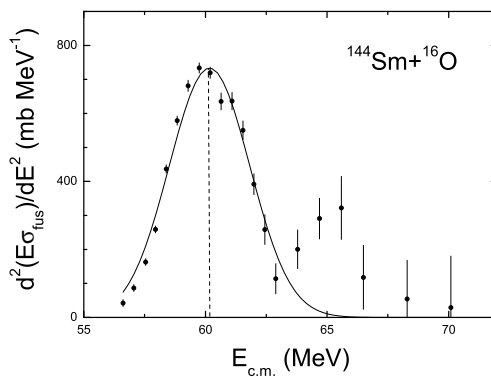


Fig. 6. Fusion barrier distribution for the $^{16}\text{O} + ^{144}\text{Sm}$ reaction, taken from Ref. [12] as an example illustrating the way of determination of the ‘experimental’ fusion barrier (see text). Solid line is a Gaussian fitted to experimental points. We take position of the maximum (dashed line) as the ‘experimental’ fusion barrier.

Gaussian, and define the ‘experimental’ fusion barrier to be the energy corresponding to position of the maximum. In such a way, we have determined the ‘experimental’ fusion barriers for different projectile-target combinations and compared them with predictions of our model.

The comparison (see Fig. 7) is presented for a number of medium and heavy systems, for which the barrier heights range from 60 to about 120 MeV. It is seen that the interaction barriers, calculated within our model, agree very well with the experimental fusion barriers. One can notice however that the theoretical barriers are slightly but systematically higher than the experimental values (on the average, by about 1 MeV). Considerably larger differences (up to 8 MeV for heaviest systems included in Fig. 7) are seen for the interaction barriers calculated with the latest version of the proximity potential [19].

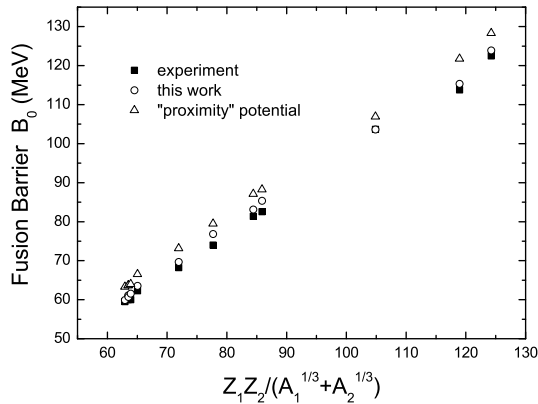


Fig. 7. Comparison of experimental values of the fusion barrier (deduced from the measured fusion barrier distributions [12–18]) with results of this work, and also with predictions based on recent version of the proximity potential [19].

5. Conclusions

We propose a scheme of calculating potential energy of mono- and/or di-nuclear systems in the configurational space of deformation and mass asymmetry degrees of freedom. This scheme can be applied for description of fusion reactions, damped collisions, and also fission reactions.

We performed extensive tests of our method of calculations by using experimental data on both, fission- and fusion barriers. This provided a consistent, complementary tool of verification of the proposed method throughout the entire potential energy surface. We can now use our model with confidence in various applications. For example, we found that our dynamical

cal calculations of nucleus-nucleus collisions, based on one-body dissipation model (see *e.g.* Ref. [20]) led to much better agreement with experimental data when we applied the new method of calculating the potential energy. An example of such dynamical calculations is shown in Fig. 8. We calculated dynamical trajectories for the reaction $^{86}\text{Kr} + ^{166}\text{Er}$ studied experimentally at an energy of 8.18 MeV/nucleon [21]. The classical ‘dissipative deflection function’ obtained assuming the one-body-dissipation Rayleigh force is shown in Fig. 8 by dashed line that perfectly follows the ridge in the landscape of the double differential cross section, $d^2\sigma/(d\Theta dE)$, in the ‘Wilczynski plot’ for the studied reaction. This fact can be interpreted that both, conservative and dissipative forces have been calculated correctly. It should be emphasized here that the process of ‘dissolving’ of nuclear structure in the transition region from the di-nuclear to mono-nuclear regime plays especially important role for trajectories leading to the grazing angle and for slightly smaller impact parameters. We plan therefore to carry out systematic calculations of the dissipative deflection functions in order to confirm our method of calculating the potential energy surface in the transition region, and then to use those calculations as a tool for detailed studies of the dynamical range of the mechanism of one-body dissipation.

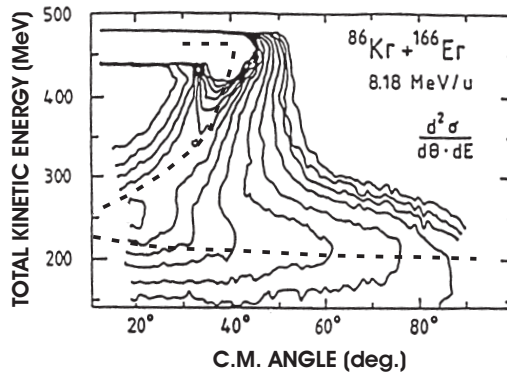


Fig. 8. Contour diagram of the double differential cross section, $d^2\sigma/(d\Theta dE)$ in the $^{86}\text{Kr} + ^{166}\text{Er}$ reaction [21], as a function of the scattering angle and the total kinetic energy, compared with the ‘dissipative deflection function’, (dashed line) calculated assuming one-body dissipation. Adapted from Ref. [21].

We would like to thank W.J. Świątecki for many illuminating discussions. This work was supported by the Polish State Committee for Scientific Research (KBN), Grant No. 2P03B05419.

REFERENCES

- [1] L. Shvedov, J. Błocki, J. Wilczyński, *Acta Phys. Pol. B* **33**, 439 (2002).
- [2] H.J. Krappe, J.R. Nix, A.J. Sierk, *Phys. Rev.* **C20**, 992 (1979).
- [3] J. Błocki, W.J. Świątecki, Nuclear Deformation Energies, Preprint LBL-12811, Berkeley, 1982.
- [4] K.T.R. Davies, J.R. Nix, *Phys. Rev.* **C14**, 1977 (1976).
- [5] W.D. Myers, W.J. Świątecki, *Table of Nuclear Masses according to the 1994 Thomas–Fermi Model*, Preprint LBL-36803, Berkeley, 1994.
- [6] W.D. Myers, W.J. Świątecki, *Ark. Fys.* **36**, 343 (1966).
- [7] J. Randrup, *Ann. Phys. (N.Y.)* **112**, 356 (1978).
- [8] L.G. Moretto, S.G. Thompson, J. Routti, R.C. Gatti, *Phys. Lett.* **B38**, 471 (1972).
- [9] A. Grewe *et al.*, *Nucl. Phys.* **A614**, 400 (1997).
- [10] H. Weigmann, in *The Nuclear Fission Process*, ed. C. Wagemans, CRC Press, 1991, p. 30.
- [11] N. Rowley, G.R. Satchler, P.H. Stelson, *Phys. Lett.* **B254**, 25 (1991).
- [12] J.R. Leigh *et al.*, *Phys. Rev.* **C52**, 3151 (1995).
- [13] D.J. Hinde *et al.*, *Phys. Rev.* **C53**, 1290 (1996).
- [14] J.C. Mein *et al.*, *Phys. Rev.* **C55**, R995 (1997).
- [15] C.R. Morton *et al.*, *Phys. Rev.* **C52**, 243 (1995); **C60**, 044608 (1999).
- [16] D.J. Hinde *et al.*, *Phys. Rev.* **C60**, 054602 (1999).
- [17] C.R. Morton *et al.*, *Phys. Lett.* **B481**, 160 (2000).
- [18] F. Scarlassara *et al.*, *Nucl. Phys.* **A672**, 99 (2000).
- [19] W.D. Myers, W.J. Świątecki, *Phys. Rev.* **C62**, 044610 (2000).
- [20] J. Błocki, O. Mazonka, J. Wilczyński, Z. Sosin, A. Wieloch, *Acta Phys. Pol. B* **31**, 1513 (2000).
- [21] A. Gobbi, W. Nörenberg, in *Heavy Ion Collisions*, ed. R. Bock, North Holland Publ. Co., 1980, Vol. 2, p. 127.